3D modelling of a multi pass dissimilar tube welding and post weld heat treatment of nickel based alloy and chromium steel

Ram Kumar-Krishnasamy*, Dieter Siegele

Fraunhofer Institute for Mechanics of Materials

Wöhlerstraße 11, 79108 Freiburg, Germany

Abstract

A dissimilar tube welding is performed between the nickel based Alloy617 and creep resistant steel VM12 using the former as the weld material. SYSWELD welding software is used to model the thermal and mechanical analysis. A readily available thermal history is used to calibrate the heat source input for the thermal analysis to generate the adequate thermal cycle by fitting the welding velocity, heat intensity factor of the GOLDAK heat source and the length of molten zone. The transient temperature field is then incorporated as the input for the mechanical analysis to obtain the residual stresses in which the phase transformation of the materials during welding is taken into account. Subsequently, the weld materials are characterized by using the Norton's creep law to determine the Norton parameters based on relaxation experiments. The residual stresses generated after the multi pass welding by SYSWELD is transferred into the ABAQUS as the initial condition for the post weld heat treatment (PWHT) simulation. The simulations show that the residual stresses reduce in magnitude but still present even after PWHT.

1. Introduction

The residual stresses introduced by welding are of major concern in the safety and reliability of components especially on those operating at high temperatures and imposed by complex loads. The influence of creep, fatigue and thermomechanical behaviour of welds plays a decisive role in the lifetime of engineering components. In general, the residual stresses generated during the fabrication and welding lead the weld and the neighbouring heat affected zone to be the most critical parts of welded tubes applied in power plants [1]. Especially, in multi pass welding the residual stress patterns reflect a complex thermal history of the weld region.

Corresponding author.Tel:+49 761 5142 237 fax: +49 5142 401

E-mail address: ram.kumar.krishnasamy@iwm.fraunhofer.de

In this case, the microstructure, residual stresses, and distortion are altered with each applied weld pass. Moreover, welding dissimilar tubes introduce additional complexity due to varying temperature dependent material properties of base and weld metal [2]. Therefore, the investigation of these residual stresses is vital for determination of the fatigue lifetime as well as the damage behaviour of such welded tubes.

In this work a 3D multi pass welding simulation is performed between dissimilar tubes, namely the nickel based Alloy617 and creep resistant steel VM12 using the former as the weld material. In the first part, the temperature field is calculated by a thermal finite element analysis where the temperature profile at the surface is adapted to the experimental thermal history. In the second part, the mechanical analysis is performed using the thermal history from the first part as the input to simulate the residual stresses.

For the present investigation, residual stresses after welding and after post weld heat treatment are determined using the finite element method. Commercial software SYSWELD is used to perform the thermal and mechanical calculations in welding. The residual stresses generated after the multi pass welding by SYSWELD is transferred into ABAQUS as the initial condition for the PWHT simulation. The numerically simulated residual stresses directly after welding and the reduction after PWHT are compared at various locations.

2. Welding procedure

The dissimilar tubes were welded manually by a welding expert in ALSTOM Power Stuttgart. Figure 1 shows the set up for the dissimilar welding of the tubes. The Alloy617 side of the tube was clamped. Before the welding process, the region close to the weld of the Alloy617 and the VM12 tubes were heated up to 200^0 C. Two weld points were made between the tubes to hold the tubes together before the hand welding took place. The welds were divided into 3 parts. First four roots welds (WL) were welded followed by four intermediate welds (ZL) and finally 8 cover welds (DL) completed the welding process. Thermocouples were located on both sides of the tubes for the measurement of the thermal cycles. The welding sequence as described above is shown in Figure 2.

3. Modelling of the dissimilar welding process

Modelling a welding process is a complex task. This is evident because the numerical simulation of the residual stresses and distortions needs to accurately take into account the interactions between heat transfer, metallurgical transformations and mechanical fields [2].

3D finite element model is developed in order to accurately capture the temperature fields and the residual stresses in the dissimilar welded tubes. Since the dimensional changes in welding are negligible and mechanical work done is insignificant compared to the thermal energy, a sequential formulation is opted to characterize the thermomechanical behaviour of the welded tubes during welding [3].

In the first step, the temperature distribution and its history in the welding model are computed by a heat conduction analysis. Then, the temperature history is employed as a thermal load in the subsequent mechanical elastic plastic calculation of the residual stress field. Although the heat conduction problem is solved independently from the stress problem, the formulation considers the contributions of the transient temperature field to the stress analysis through thermal expansion, as well as temperature-dependent thermo-physical and mechanical properties.

The temperature dependent thermal physical constants are taken from literature as well as material data sheets [4] [5]. Elastic-plastic material properties and isotropic hardening are assumed. The parameters (Young's modulus, Poisson's ratio, yield stress, strain hardening) are temperature dependent and also taken from literature [4] [5]. For temperatures higher than those provided in references, the parameters are extrapolated linearly with temperature [3] [6].

The thermal physical properties and mechanical properties of the base materials are shown in Table 1a-b. The nickel based Alloy617 is also used as the weld material.

4. Computational Welding Simulation

The welding simulation is performed based on the original welding sequence during the hand welding. For the multi pass welding, an element activation technique is used to introduce the single welds with reference to the welding time from the experimental thermal cycles. A moving heat source is then travelled along the circumference of this weld to generate the thermal cycles. This heat is described in section 4.1.2. The welded tubes at sequence are shown in Figure 3a-3c after the completion of root, intermediate and cover welds. The length, outer diameter and the thickness of the completely welded tube model are 100mm, 38mm and 6.3mm.

The locations of thermocouples on both sides of the tubes are shown on the Figure 4. Based on the thermal history captured at the thermocouple TE3 from the experiment, the simulation is adapted for the complete multi pass welding. The accuracy of this method is later controlled for the remaining thermocouples on both sides of the tubes.

4.1 Thermal Analysis

The theoretical background for the welding simulation is given below. The equations employed by SYSWELD during the thermal and mechanical analysis are described briefly [7].

The transient heat transfer equation for welding is given by

$$\rho c \frac{\partial T}{\partial t}(x, y, z, t) = -\nabla \cdot \vec{q}(x, y, z, t) + Q(x, y, z, t) \qquad \text{Equation 1}$$

where ρ is the density of the materials, c is the specific heat capacity, T is the current temperature, $\vec{q}$ is the heat flux vector, Q is the internal heat generation rate, x, y and z are the coordinates in the reference system, t is the time, and ∇ is the spatial gradient operator.

The non-linear isotropic Fourier heat flux constitutive equation is employed:

$$\vec{q} = -k\nabla T$$ Equation 2

where k is the temperature - dependent thermal conductivity.

4.1.2 Heat Source

In this study, the heat from the moving welding arc is applied as a volumetric heat source with a double ellipsoidal distribution proposed by Goldak [8]. The front half of the source is the quadrant of one ellipsoidal source and the rear half is the quadrant of another ellipsoid. In this model, the fractions f_f and f_r of the heat deposited in the front and rear quadrants are needed, where $f_f + f_r = 2$.

The power density distribution inside the front quadrant becomes:

$$q(x,y,z,t) = \frac{6\sqrt{3} f_f Q}{abc\pi\sqrt{\pi}} e^{-3x^2/a^2} e^{-3y^2/b^2} e^{-3[z+v(\tau-t)]^2/c^2}$$ Equation 3

Similarly, for the rear quadrant of the source the power density distribution inside the ellipsoid becomes:

$$q(x,y,z,t) = \frac{6\sqrt{3} f_r Q}{abc\pi\sqrt{\pi}} e^{-3x^2/a^2} e^{-3y^2/b^2} e^{-3[z+v(\tau-t)]^2/c^2}$$ Equation 4

To perform a welding simulation, a reference line, welding trajectory line, start and end nodes as well as the start elements are needed. The weld line must be situated on the skin of the material, in the centre of the molten material. Else an offset is needed. Based on the welding velocity and the length of molten zone together with the welding trajectories, the parameters a, b, c are automatically generated by SYSWELD. The total absorbed power then needs to be fitted with an intensity function during the thermal analysis.

Both the thermal radiation and heat transfer on the weld surface are assumed. Radiation losses are dominating for higher temperatures near and in the weld zone, and convection losses for lower temperatures away from the weld zone [8] [9].

The heat transfer equations involved during welding simulations are described more intensively in various literatures [8] [9].

4.2 Mechanical Analysis

The mechanical analysis is based on the equations describing the static equilibrium. As the plastic dissipation is neglected in the thermal analysis, thermal and mechanical analysis can be treated successfully. Thus the mechanical calculation is achieved using the temperature fields computed previously by the thermal analysis.

During the welding process, the solid-state phase transformation occurs in both the materials especially at the HAZ. When the steel is heated above the T_{AC1} temperature, its body centred cubic structure starts to transform to a face centred cubic structure, and the volume decreases [10]. During rapid cooling, the austenite with face centred cubic structure changes to martensite with a body tetragonal structure, and the volume increases. Therefore the effects on the residual stress of volume change and the yield stress change due to martensite transformation were taken into account. The phase transformation effect is incorporated through the temperature dependant material properties during the mechanical analysis. However, transformation induced plasticity was not taken into account. Ignoring this component, the strain increment can be expressed by the following equation [9]:

$$\Delta\varepsilon = \Delta\varepsilon^{E} + \Delta\varepsilon^{P} + \Delta\varepsilon^{T} + \Delta\varepsilon^{\Delta V} \qquad \text{Equation 5}$$

5. Post Weld Heat Treatment

The residual stresses generated after the multi pass welding by SYSWELD is transferred into the ABAQUS as the initial condition for the PWHT simulation.

The heat treatment of the welded tube is performed by introducing a tempering temperature of 760°C for a time range of 30 min. Conditioned by the heating and cooling period the tube undergoes a long dwell time at high temperature which causes to additional creep of the material and contributes to the reduction of the residual stresses.

5.1 Weld Material Characterization through Relaxation Tests

For the simulation of PWHT, besides the stiffness values, the creep properties of the material being examined were needed. To characterize these properties, relaxation tests were carried out at high temperatures taking into account the temperature spectrums of the PWHT process. The specimens were first strained on a servohydraulic machine till it reaches an intended axial stress (120MPa till 200MPa). Subsequently, with the help of an extensometer, the axial strain on the specimen was held constant and the relaxation of the axial stresses was continually measured. These tests were carried out at constant temperatures of 550°C, 625°C and 760°C. The specimens were tested both Alloy617 and VM12 for the temperatures mentioned above. The relaxations curve from the experiments for both the materials for the temperature of 550 °C (VM12) and 760 °C (Alloy617) are shown exemplarily in Figure 5.

The relaxation and creep properties are numerically modelled based on the Norton's creep law. The parameters for this law are obtained from the relaxation test performed at various temperatures and stresses.

The Norton [11] power law used for the characterization of the materials is given below:

$$(\dot{\varepsilon})_{II} = A(\sigma)^n \qquad \text{Equation 6}$$

Where A and n are material constants

In Figure 5, besides the experimental relaxation curves, the numerically generated stress relaxation curves based on Norton's creep law are also plotted.

6. Results and Discussions

6.1 Welding Temperature Cycles

As mentioned in section 4, for the thermal analysis, the heat source fitting is done only for thermocouple TE3 (2.75mm from the weld axis) and the reliability of the fitting is controlled for the other thermocouples. After the completion of the thermal analysis, the thermal cycles for the complete tube are analyzed for all other thermocouples based on the nodal temperatures captured during the simulation. It was found that, despite the fact

that hand welding could lead to high discrepancy, the simulated thermal cycles have an excellent match with those of the experimental ones.

Figures 8- 9 shows for example the thermal cycles captured on the root welds on VM12 side and intermediate welds on Alloy617 side.

VM12Side

Both TE8 and TE10 show an excellent agreement with the experimental results. For TE9, there is a slight discrepancy in the peak temperatures. However, for all TE8, TE9 and TE10, it is obvious that the heating and cooling rates are in good match with the experiment. This is an important observation since these rates are very decisive for the generation of residual stresses. Similar results are obtained for the intermediate and cover welds.

Alloy617 Side

All the TE3, TE4 and TE5 have shown an excellent match between the simulated and experimental thermal cycles. The peak temperatures as well as the heating and cooling rates are in a good agreement. The slightest difference between the temperatures during the last past of the cooling curves is negligible [9] since these temperatures are way below the $T_{8/5}$ of the material.

6.2 FE Residual Stress Distribution

The residual stresses after welding and PWHT are shown in Figure 8 and Figure 9. As an example, the axial residual stresses are shown on the outer surface of the dissimilar tubes and the hoop residual stresses are shown in sections through the dissimilar tubes. High residual stresses arise at interface between the VM12 and the weld material after welding. The magnitude of the residual stresses is typical for dissimilar welds [3]. However, no residual stress measurements are available for validation of the results. In general, after PWHT the stresses relax but still remain in the tubes.

The residual stresses along the circumference of the tubes are investigated at 90° and -90° with respect to the welding starting position (Figure 10). Here, half of the weld seams have been deposited and therefore taken as a representative location for comparison of residual stresses. The distributions of the hoop and axial stresses directly after welding and after PWHT at 90° and -90° with respect to the welding starting position [12] are shown in Figure 11 till Figure 14.

Figure 11 and Figure 12 show significant reduction in hoop stresses on the VM12 after PWHT. However, the stresses are not completely reduced. On the Alloy617 side, the hoop stresses show only marginal reduction after PWHT. However, away from the weld there stresses are almost consistent on both VM12 and Alloy617 sides.

Figure 13 and Figure 14 show that the axial stresses are only reduced significantly at -90° on VM side. On the contrary, residual stress reduction is more visible at 90° on the Alloy617 side. Similar to the hoop stresses, away from the weld there stresses are almost consistent on both VM12 and Alloy617 sides after PWHT.

In general, the calculated residual stresses show a large variation along the circumference due to the weld sequences and slope-ins and slope-outs at the different angles. Besides the repetitive heating and cooling of the weld area during the multi pass welding, the inhomogeneous stress distribution is mainly contributed by the dissimilar material properties especially the coefficient of heat expansion and thermal conductivity.

Conclusions

In this study, 3D FE model is developed to analyze the temperature fields and the residual stress distributions for a multi pass welding of dissimilar parent materials. The effect of the PWHT on the welded tubes was observed by comparing the residual stresses directly after the welding and after annealing the welded tubes. The proposed computational procedure is an effective method for predicting the thermal cycles and the welding residual stresses. According to the simulated and experimental results, the following conclusions can be drawn:

(1) Based on the simulated results of the 3D model, a temperature distribution could be modelled using the GOLDAK moving heat source which reproduces the experimental heat input into the model even for the dissimilar tubes.

(2) In the present study, both the welding simulation and the PWHT predicted satisfying residual stress distribution and reduction. Though, no residual stress measurements available for validation, the magnitude of the residual stresses is typical for dissimilar welds. Measurement of residual stresses after welding and PWHT at various locations would be an excellent validation for future work.

(3) By using such models, the temperature fields and residual stresses can be predicted for dissimilar tubes. The model can be modified to study the effect of various parameters on the residual stresses such as the

welding velocity, length of molten zone, heating and cooling time. In addition the model also allows the modification of parent and weld materials. This can give a good benchmark for future welding experiments as well as selection of materials for welding. Furthermore, the model could be used for studying the effect of various annealing conditions on the reduction of the residual stresses.

Acknowledgements

This research work is part of the German contribution to the European COST536 Action »Alloy Development for Critical Components of Environmentally Friendly Power Plants«. It was also funded by the German Federal Ministry of Education and Research. The author wishes to express his gratitude to the above mentioned organizations for their financial support and the fruitful technical discussions.

References

[1] Leggat R H. Residual stresses in welded structures. International Journal of Pressure Vessels and Piping 2008; 85(3):144-151.

[2] Duranton P, Devaux J,Robin V, Gilles P, Bergheau J M .3D modelling of multipass welding of a 316L stainless steel pipe. Journal of Materials Processing Technology 2004; 153-154: 457-463.

[3] Deng D and Murakawa H.Numerical simulation of temperature field and residual stress in multipass welds in stainless steel pipes and comparison with experimental measurements. Computational material Science2006;37:269-277

[4] ThyssenKrupp VDM Material Data Sheet No.4019 - Alloy 617, Edition July 1994.

[5] Stahlschlüssel, Material Data Sheet No 1.4922 - VM12 Edition 2004.

[6] Yaghi A H, Hyde T H, Becker A A and Sun W. Finite element simulation of welding and residual Stresses in a P91 steel pipe incorporating solid-state phase tzransformation and post-weld heat treatment, J. Strain Analysis 2008, Vol.43:275-293

[7] SYSWELD Welding Handbook 2008:ESI GmbH

[8] Goldak J, Chakravarti A, Bibby A. A new finite element model for welding heat sources. Metallurgical and Materials Transactions 1984; B(15):299-305

[9] Radaj D.: Heat effects of welding, temperature field, residual stress and distortions, Springer, 1992.

[10] Koistinen D, Marburger R E. A general equation prescribing the extent of the austenite-martensite transformation in pure iron-carbon alloys and plain carbon. Michigan, 2003

[11] Norton F H . The Creep of Steel at High Temperatures 1929: McGraw-Hill, London.

[12] Krishnasamy R K, Friedman V, Squaizer Y, Siegele D. COST536 Annual Report 2008

Table1: Thermal Physical properties and Mechanical properties of Alloy617

Temperature (°C)	Specific Heat (J/kg.K)	Thermal Conductivity (W/mm.K)	Density (kg/mm^3)	Coefficient of Thermal Expansion ($°C^{-1}$)	Yield Stress (MPa)	Young's Modulus (MPa)	Poisson's ratio
20	420	0.0134	8.36E-06	1.00E-05	300	212000	0.3
100	440	0.0147	8.34E-06	1.16E-05	270	206000	0.3
200	465	0.0163	8.30E-06	1.26E-05	230	201000	0.3
300	485	0.0177	8.27E-06	1.31E-05	220	194000	0.3
400	515	0.0193	8.23E-06	1.36E-05	210	188000	0.3
500	545	0.0209	8.19E-06	1.39E-05	200	181000	0.3
600	565	0.0225	8.16E-06	1.40E-05	190	173000	0.3

Table2: Thermal Physical properties and Mechanical properties of VM12

Temperature (°C)	Specific Heat (J/kg.K)	Thermal Conductivity (W/mm.K)	Density (kg/mm^3)	Coefficient of Thermal Expansion ($°C^{-1}$)	Yield Stress (MPa)	Young's Modulus (MPa)	Poisson's ratio
20	439	0.0240	7.81E-06	1.02E-05	450	218000	0.28
100	474	0.0244	7.79E-06	1.05E-05	420	213000	0.28
200	498	0.0248	7.76E-06	1.09E-05	405	206000	0.28
300	517	0.0251	7.74E-06	1.13E-05	392	198000	0.28
400	538	0.0256	7.71E-06	1.16E-05	372	190000	0.28
500	564	0.0261	7.68E-06	1.20E-05	340	180000	0.30
600	598	0.0264	7.64E-06	1.22E-05	248	167000	0.32

Figure 1: Dissimilar tube welding setup

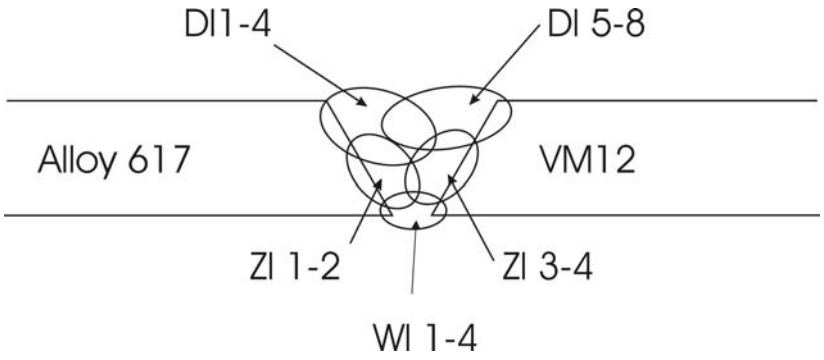

Figure 2: Welding sequence

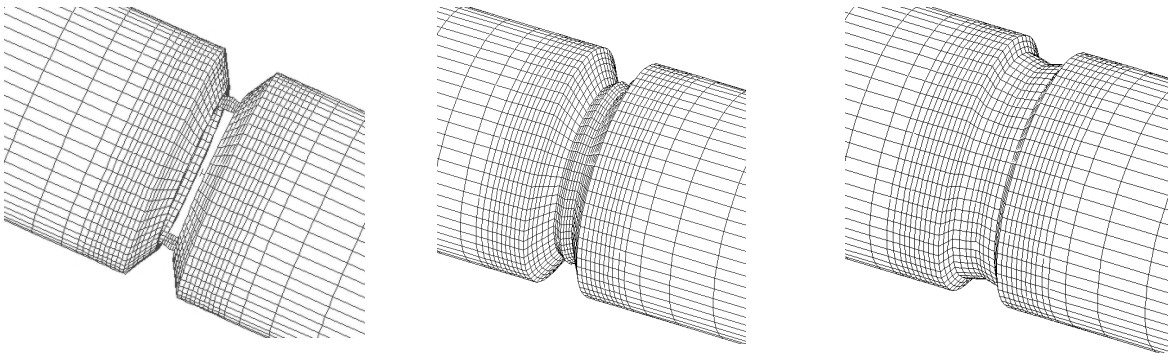

a) b) (c)

Figure 3: 3D-model of pipes with activated welds, a) weld spots, b) root welds, c) intermediate welds

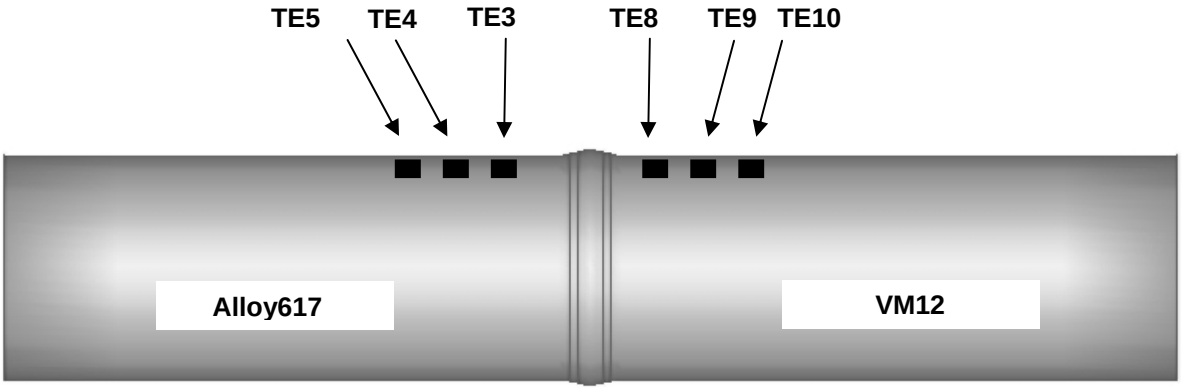

Figure 4: Thermocouples for temperature measurements

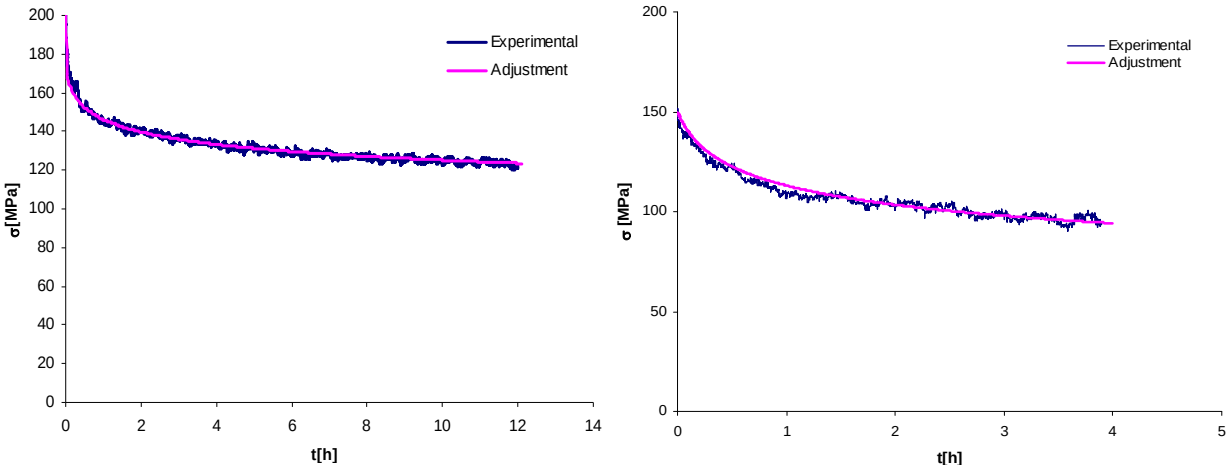

Figure 5: Model adjustment for stress relaxation; left: VM12, 550 °C; right: Alloy617, 760 °C

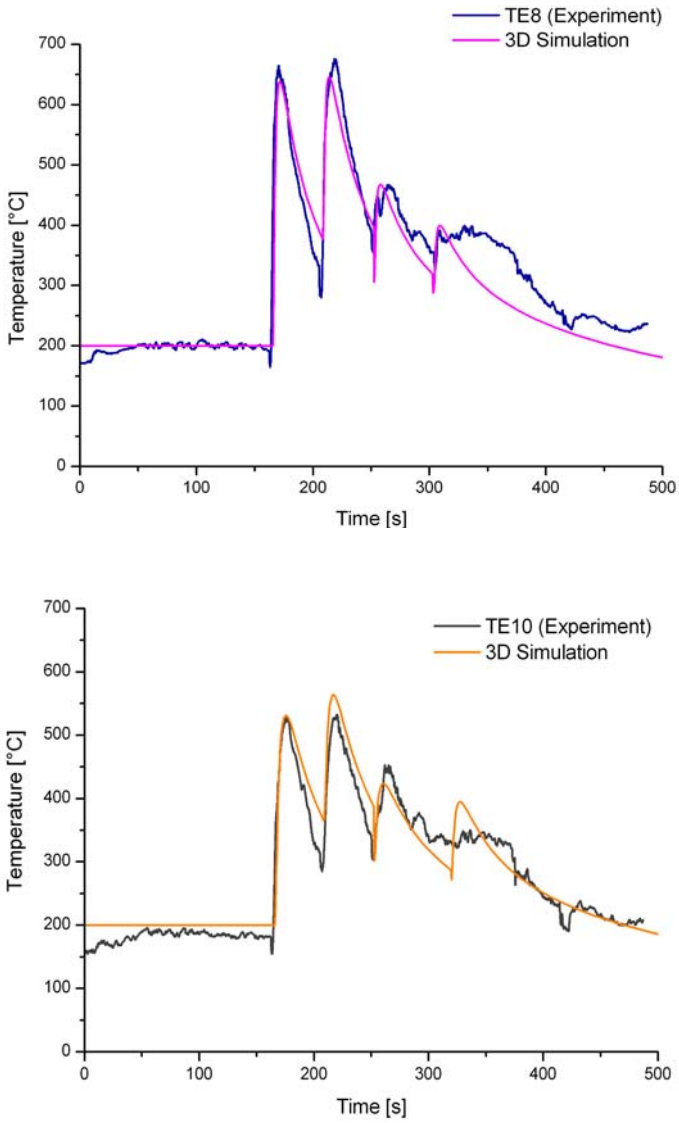

Figure 6: Thermal cycles at root welds for TE8 and TE10 (VM12)

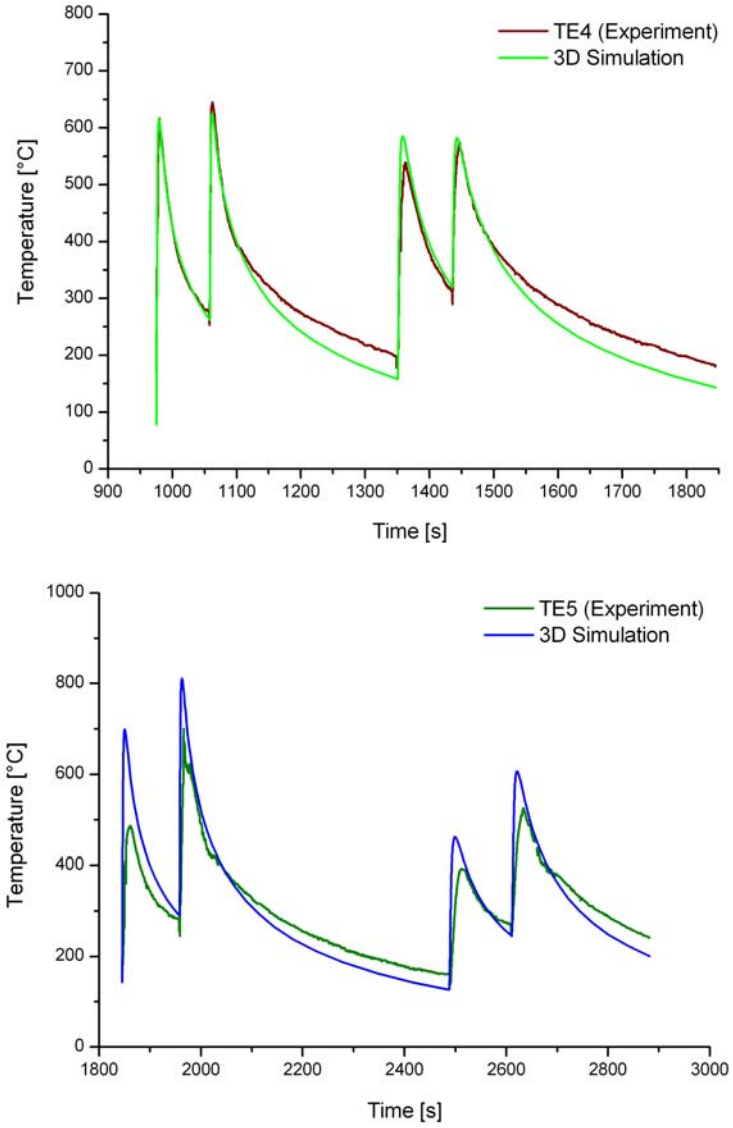

Figure 7: Thermal cycles at intermediate welds for TE4 and TE5 (Alloy617)

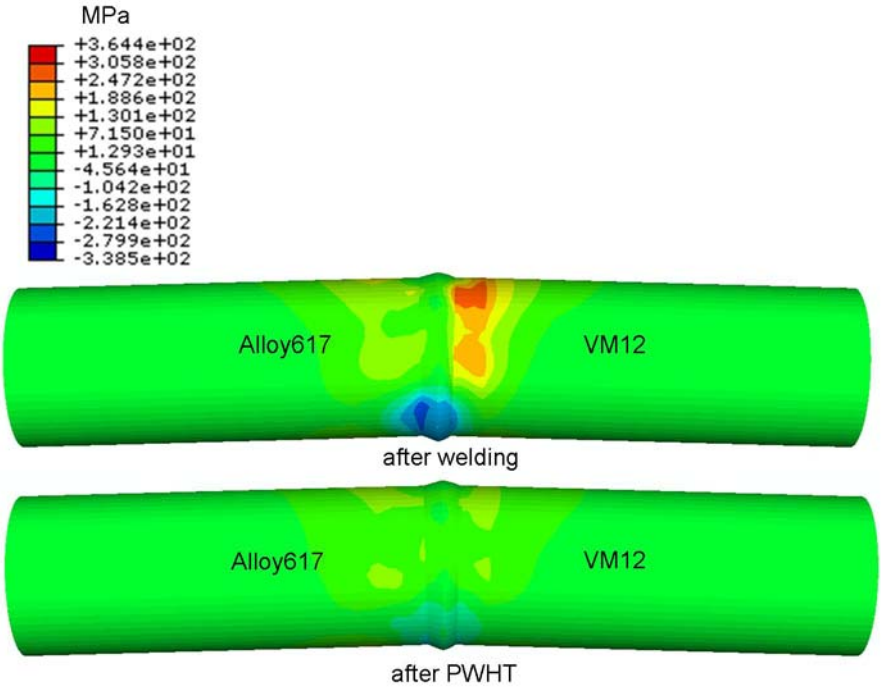

Figure 8: Axial residual stress distribution on the outer surface of the tubes

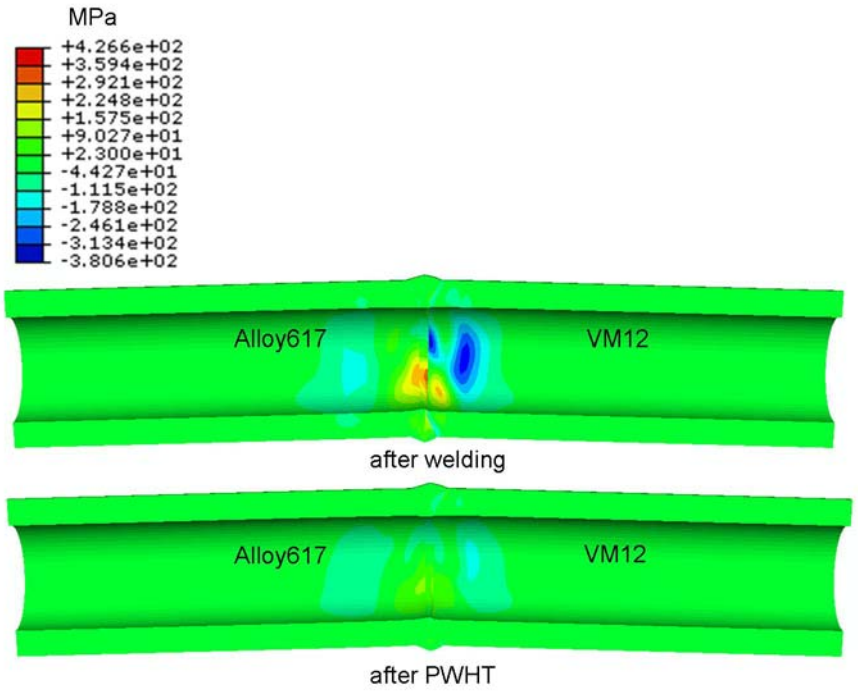

Figure 9: Hoop residual stress distribution on the sectional cut

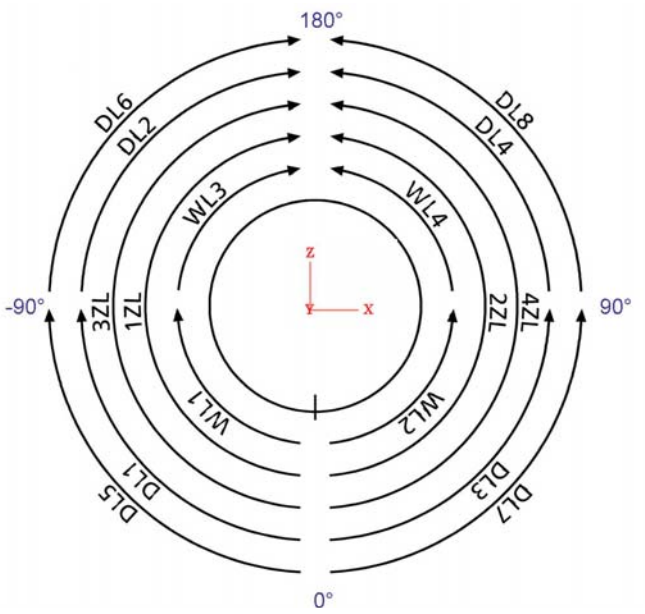

Figure 10: Positions of residual stress analysis with respect to welding start point (0°)

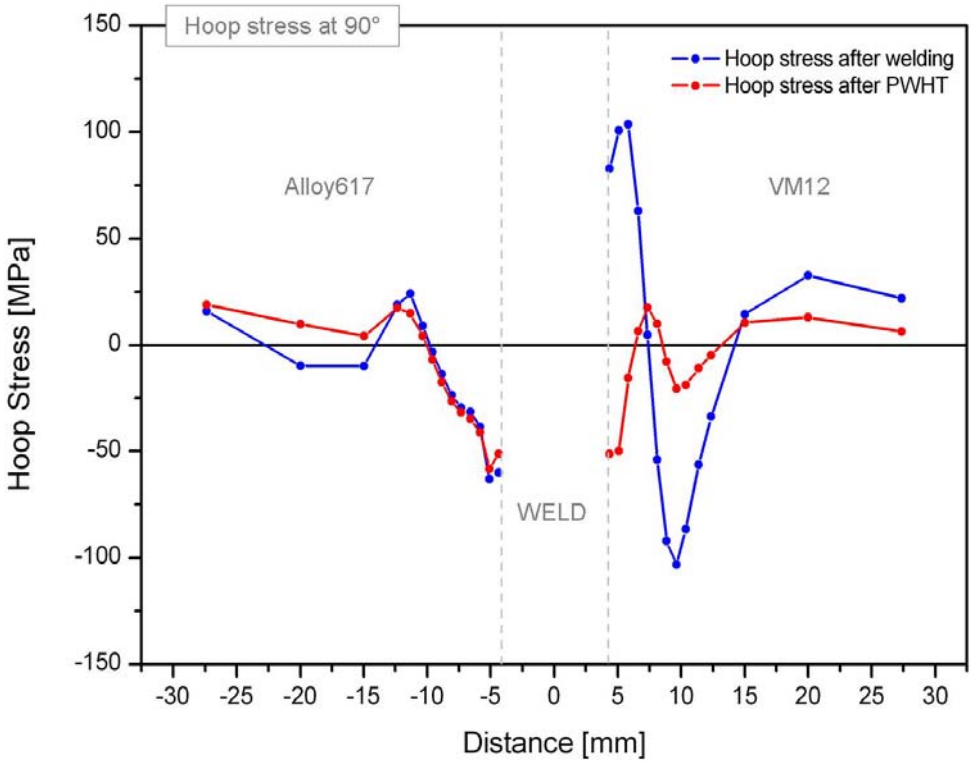

Figure 11: Hoop residual stress at 90° from weld start point

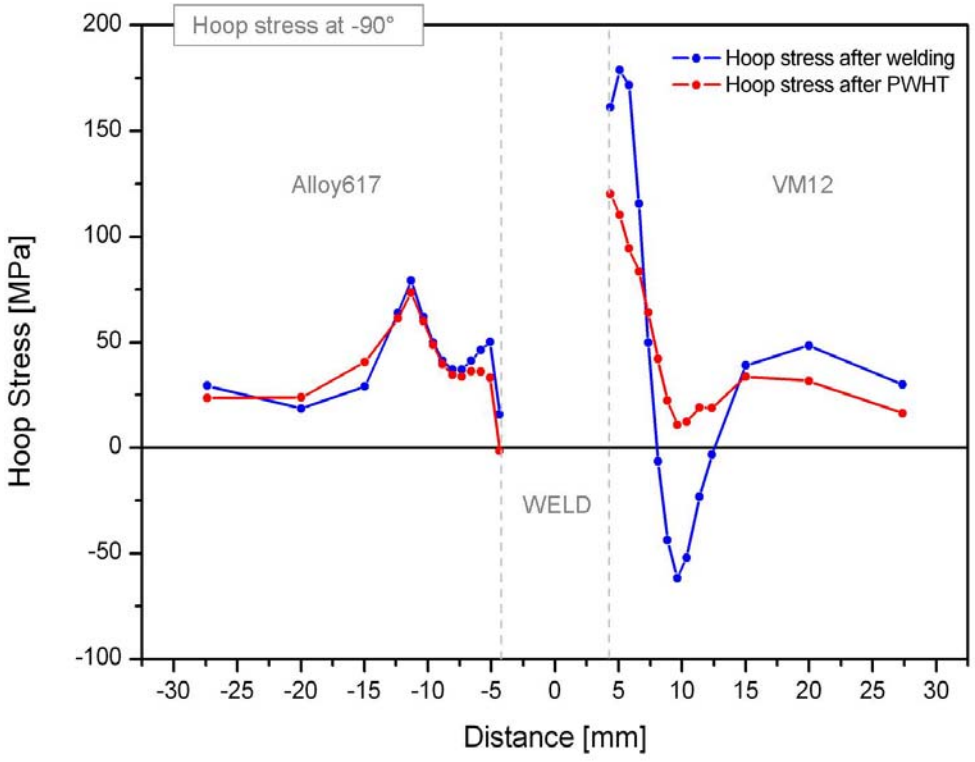

Figure 12: Hoop residual stress at -90° from weld start point

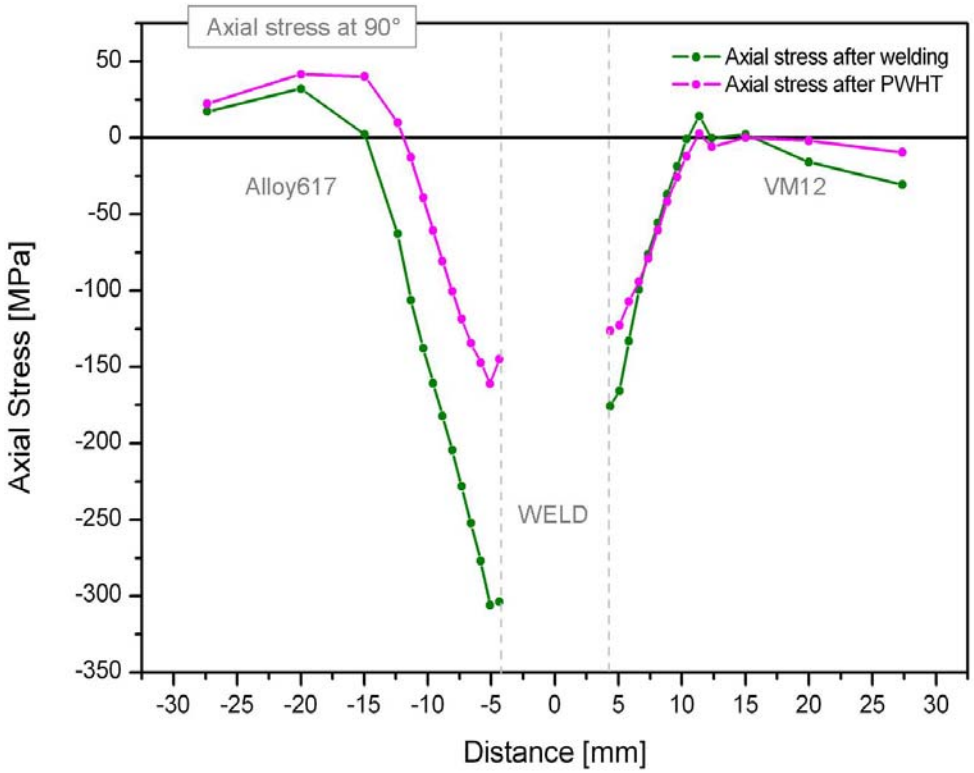

Figure 13: Axial residual stress at 90° from weld start point

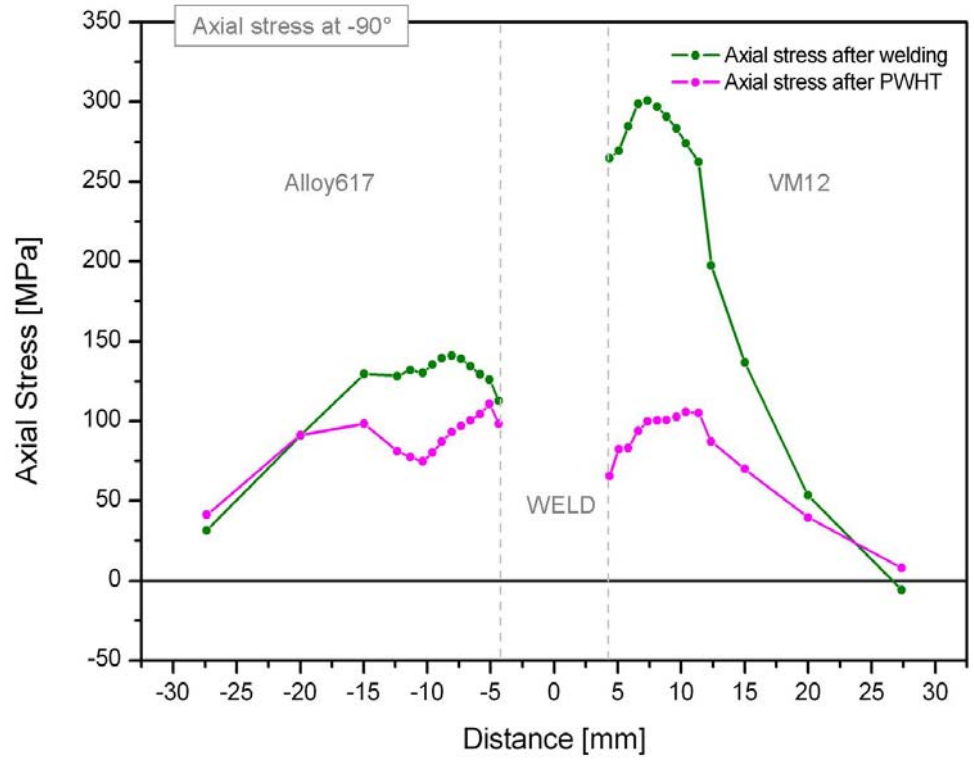

Figure 14: Axial residual stress at -90° from weld start point